The BC87 Dataset: Application of Hypothetical Event Analysis on Distorted GDS Response Functions and Some Thin Sheet Modelling Studies of the Deep Crustal Conductor

Patricia RITTER and Oliver RITTER

Department of Geology and Geophysics, University of Edinburgh, Edinburgh EH9 3JW, Scotland, U.K.

Galvanic distortion of the regional MT responses was inferred from the analyses of the BC87 dataset presented at the MT-DIW1 in 1992. Since perturbation currents also produce an anomalous magnetic field, the GDS response functions were suspected to be distorted in the long period range. In order to reveal the correct regional strike direction, hypothetical event analysis was applied to the data from all sites. With this technique, common regional information, such as strike and impedance phase, can be recovered from distorted response functions. Although the BC87 GDS data are noisy, and the distortion is more of an inductive than of a purely galvanic nature, the resulting regional strike direction of 60° agrees well with the azimuth suggested from previous MT decomposition methods.

Thin sheet modelling studies of the geometry of the deep crustal conductor (L-shaped or oblique) at 1000 s imply that along the BC87 profile induction arrows are generally produced by current concentrations around a resistive region associated with the Nelson Batholith. Comparison of the model induction arrows with those determined from the BC87 data indicates that the model featuring the oblique, NE striking conductor (SABC) may be favoured.

1. Introduction

At the first Magnetotelluric Data Interpretation Workshop (MT-DIW1) held in Wellington in 1992, interpretation of the BC87 dataset focused mainly on the MT responses, although GDS data are available for all 27 sites in the dataset. This seemed to be for two reasons: 1. GDS data quality is not very good, especially in the long period range; 2. MT observations revealed strong 3-D effects over the whole period range. These effects were interpreted partly as 3-D induction, partly as galvanic distortion, depending on the geometry of the relevant anomalies (Eisel and Bahr, 1993; Jones *et al.*, 1993; DeGroot-Hedlin, 1995). Galvanic distortion of the electric field imposes strong effects on the magnetic field components too. Therefore distortion of the magnetic response functions must also be suspected. This phenomenon is well known in GDS, but has been examined with respect to decomposition methods only recently (Groom, 1988; Zhang *et al.*, 1993; Chave and Smith, 1994).

Magnetic distortion due to near-surface conductivity heterogeneities becomes particularly evident when the magnetic response functions are presented as induction arrows: lengths and azimuths may entirely be controlled by the local anomalous magnetic field of the shallow deviations of the regional currents. Nevertheless, one would expect that the response functions also contain information on the regional geology. We can assume that this information is common to all sites within a certain area at long periods. On the other hand, distortion is highly site-dependent. Hence the magnetic distortion problem can be formulated as a combination of site-dependent distortion parameters and contributions from site-independent regional induction processes. Zhang *et al.* (1993) and Chave and Smith (1994) used these relations to extract distortion parameters

and undistorted response functions at individual sites by solving the appropriate equation systems. The method used in our approach reveals the common, regional information simply by visualizing the whole set of response functions of a surveyed area.

Hypothetical event analysis (HEA), as a method for interpreting the output from magnetometer arrays, treats the dataset as a unit, and therefore it is most effective in recovering the common information content. If the results from HEA are presented in appropriate diagrams, site-dependent parts of the vertical magnetic field can be isolated. Ritter (1996) show that with noise-free data, and good spatial coverage of the area, it is possible to determine the regional strike direction and phases of the principal regional impedances with this technique. The response functions of the BC87 dataset do not quite meet these conditions: they have large error bars at long periods and the sites are arranged along a profile. Nevertheless, all sites were submitted to HEA in the suspected period range of distortion of 100 s–1000 s. The results are consistent throughout the whole decade, confirming a strike angle in the same range as found in previous MT analyses.

Another unsolved problem of the area is the geometrical nature of the deep crustal conductor (Jones, 1993). For the MT-DIW2 we investigated with 3-D thin sheet modelling at 1000 s, whether the form of the conductor may be determined from the induction arrows; if a resistive structure associated with the Nelson Batholith is also included into the models.

2. Theoretical Background

2.1 Magnetic distortion

Conductivity heterogeneities causing galvanic distortion are generally assumed to be near-surface and much smaller than the skin depth of the host medium. However, any anomaly produces a partly galvanic response from that period on, where the magnetic source field penetrates into the host, and induction inside the anomaly is not the only cause of electric fields. With increasing period, more and more currents that are induced in the host may be deviated into, or towards, a conductive anomaly. If the anomalous magnetic field $\mathbf{B}^a$, due to local deflections of otherwise uniform regional currents, outweighs the anomalous magnetic field, due to induction inside the anomaly, $\mathbf{B}^a$ is in phase with the regional electric field $\mathbf{E}^o$. Since this galvanic response is superimposed on the regional magnetic response, it is known as the magnetic distortion effect. Depending on the size and dimension of the body, distortion may occur at periods where the skin depth of the host is of the order of the scale-length of the distorting body (Ritter, 1996). The parameters describing magnetic distortion of the regional response function are real, frequency-independent quantities (Groom, 1988; Zhang et al., 1993). If the regional structure is 1-D, the vertical magnetic field is due to distortion only:

$$B_z^a = (D_{zx}, D_{zy})\, \mathbf{E}^o = (D_{zx}, D_{zy}) \begin{pmatrix} 0 & Z^o \\ -Z^o & 0 \end{pmatrix} \begin{pmatrix} B_x^o \\ B_y^o \end{pmatrix}. \qquad (1)$$

(D_{zx}, D_{zy}) are the vertical magnetic distortion parameters; Z^o is the regional 1-D impedance. The product $(D_{zx}, D_{zy})\underline{Z}^o$ defines the *local* magnetic response function $(\mathcal{A}^\ell, \mathcal{B}^\ell)$, where $\mathcal{A}^\ell$ and $\mathcal{B}^\ell$ denote the components in x- and y-directions, respectively. For a regional two-dimensional structure, the regional vertical magnetic field B_z^o must be considered:

$$B_z = B_z^a + B_z^o = [\,(\mathcal{A}^\ell, \mathcal{B}^\ell) + (\mathcal{A}^o, \mathcal{B}^o)\,]\, \mathbf{B}_h^o = (\mathcal{A}, \mathcal{B})\, \mathbf{B}_h^o. \qquad (2)$$

In this case, the observed response function $(\mathcal{A}, \mathcal{B})$ consists of a local and a regional part. The local part $(\mathcal{A}^\ell, \mathcal{B}^\ell)$ contains the regional 2-D impedance tensor. If the observation points are well removed from any regional lateral boundary, the regional contribution can be assumed small and homogeneous across a region of considerable extension, especially for long periods.

2.2 Hypothetical event analysis

We can calculate a predicted value for the vertical magnetic field B_z^p that is associated with a certain polarization $\vartheta^\star$ of the horizontal magnetic field from the observed response function $(\mathcal{A}, \mathcal{B})$. The horizontal field $B^\star$ is supposed to be of unit amplitude over the area of investigation. Using the above expressions which include magnetic distortion, the predicted vertical field in observation coordinates is obtained from:

$$B_z^p = \left[(D_{zx}, D_{zy}) \, \underline{\mathbf{R}}_{\theta_r} \, \underline{\mathbf{Z}}'^o \, \underline{\mathbf{R}}_{\theta_r}^T + (0, \mathcal{B}'^o) \, \underline{\mathbf{R}}_{\theta_r}^T \right] \left(\begin{array}{c} 1 \cdot \cos \vartheta^\star \\ 1 \cdot \sin \vartheta^\star \end{array} \right). \qquad (3)$$

The primes denote quantities in regional strike coordinates (x', y' with a strike direction parallel to the x'-axis) and $\underline{\mathbf{R}}_{\theta_r}$ denotes anti-clockwise rotation by the strike angle θ_r. The equation for the predicted value simplifies considerably for two special cases: when the polarization azimuth equals the regional strike direction, and when it is perpendicular to it.

$$\vartheta^\star = \theta_r : \qquad B_z^p = Z'_{yx}[-D_{zx} \sin \theta_r + D_{zy} \cos \theta_r], \qquad (4)$$

$$\vartheta^\star \perp \theta_r : \qquad B_z^p = Z'_{xy}[\ D_{zx} \cos \theta_r + D_{zy} \sin \theta_r] + \mathcal{B}'^o. \qquad (5)$$

In fact, the expression for the predicted vertical magnetic field B_z^p for the first case does not contain any contribution from the regional vertical field at all. This direction corresponds to the B-polarization, where no vertical field is generated. Note that the predicted fields at both polarizations contain only one of the principal impedances. This is an important aspect, because it implies that their phases are equal to the phases of the respective regional impedances, if the regional contribution to the vertical field is sufficiently small. In this case, the predicted values at all sites representing the same regional geology should show the same phases at a given period.

In practice, one can find the regional strike direction by gradually varying the polarization azimuth $\vartheta^\star$ and plotting the predicted values of all sites at one given period in the complex plane (Argand diagram). We can determine the regional phase when the data points fall on a line through the origin, indicating the common phase angle. This happens when the magnetic field is polarized in the strike direction of the regional structure, or perpendicular to it. If the common phase falls in the range $0° - 90°$, the response is at least partly caused by galvanic distortion, and the phase angle found is close to the respective impedance phase. If the magnetic response functions are not purely galvanic, but contain also a strong contribution from induction inside the anomaly, the distribution of the predicted values is less linear, and the phase determined by this method is negative. In that case, the phase angle found corresponds to the phase difference between the magnetic source field and the anomalous magnetic field induced in a local structure, whereas the vertical field eliminated belongs to a more regional structure. The strike direction of the latter is indicated by the polarization azimuth.

3.   The BC87 Dataset

3.1   Induction arrows (Wiese convention)

In the short and intermediate period range ($T < 10$ s) the angular distribution of the azimuths of the real arrows is very scattered along the profile. At longer periods ($T > 10$ s), however, arrows at most sites follow an overall trend, changing smoothly from $-90°$ to directions around $0°$ ($\pm 30°$) with increasing periods, although in this range magnetic response functions have relatively large errors. At these periods, the imaginary arrows point approximately $-180°$. Lengths and azimuths of the Wiese arrows are shown in Fig. 1 for periods 450 s and 910 s. Note that Wiese arrows point away from conductive regions.

The arrow directions suggest an east-west striking structure at some depth to the south of the profile. However, this does not coincide with the strike direction inferred from MT results at 45°
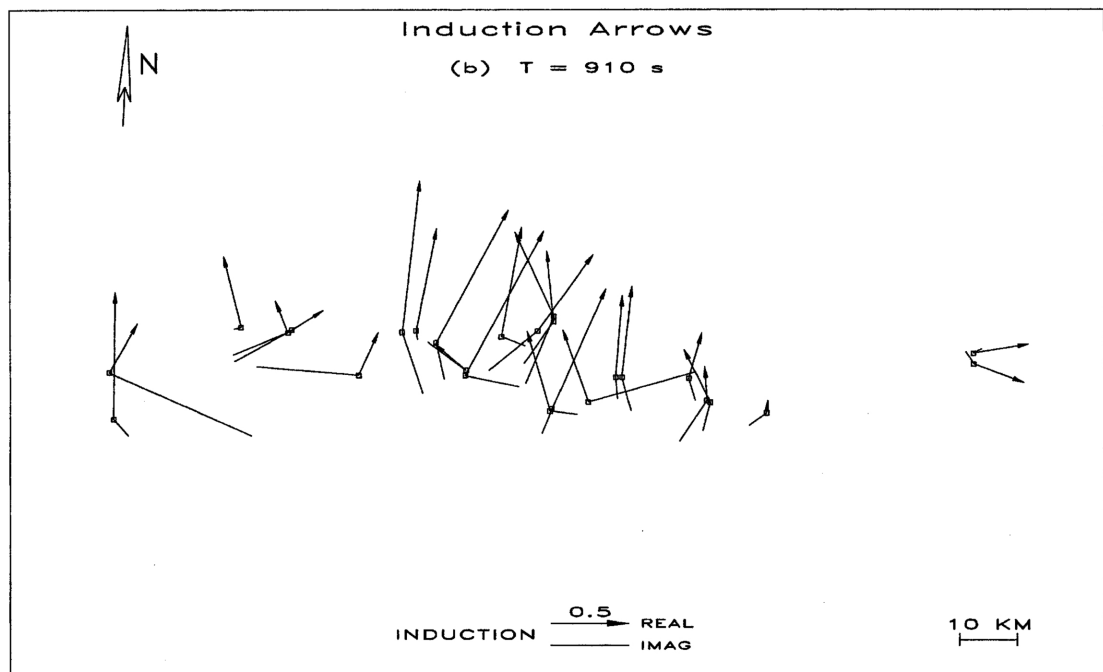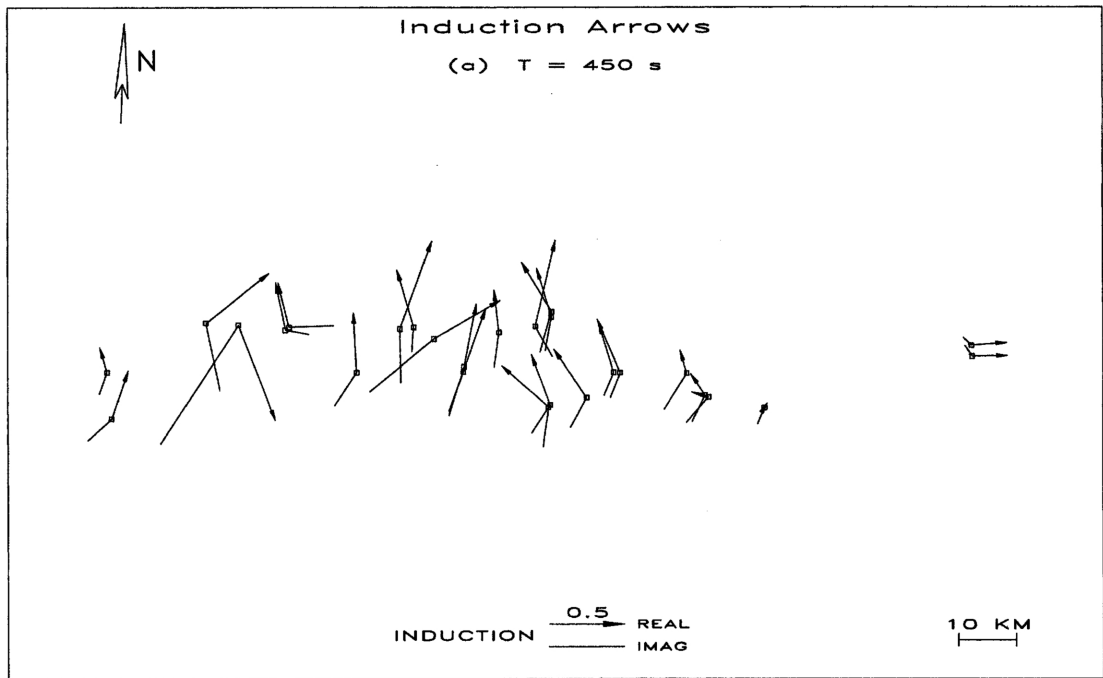
Fig. 1. Induction Arrows (Wiese convention) of all 27 sites at (a) 450 s and (b) 910 s; REAL: real arrows, IMAG: imaginary arrows.
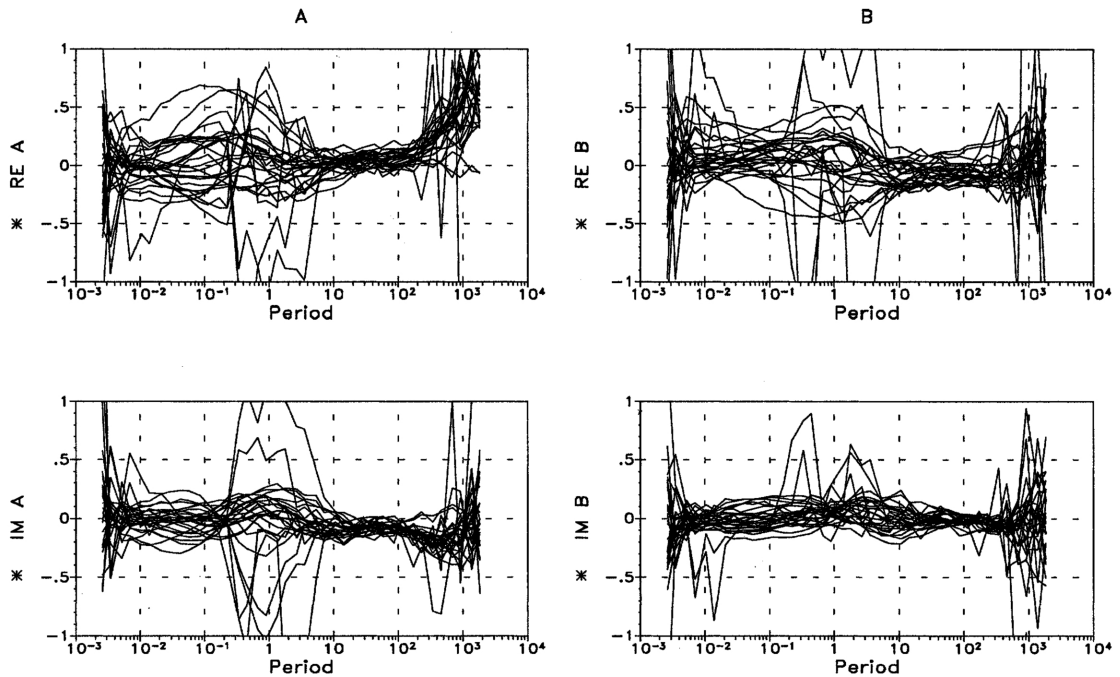
Fig. 2. Magnetic response functions (A, B) of all sites over the whole period range; RE: real parts, IM: imaginary parts.

to 60°, associated with the upper mantle anisotropy (Eisel and Bahr, 1993; Jones *et al.*, 1993). Since the amplitudes of the response functions show a definite maximum in the intermediate period range between 0.1 s and 1 s at all sites (Fig. 2), we can assume that induction takes place in the upper parts of the crust (i.e. the conductor at the eastern edge of the resistive Nelson Batholith, Jones, 1993). The large arrows at longer periods are likely to be produced by currents being deflected by these complex structures and the vertical magnetic field components observed may reflect a mixture of induction and galvanic processes.

3.2 Hypothetical event analysis

In order to find a more reliable regional strike direction, we applied HEA to all magnetic response functions in the range 10 s–1000 s. In the case of the BC87 dataset, sites are located along a profile (150 km E-W) with only limited spatial extent (25 km N-S). Hence a mapping of the results in contour plots, as it is usually undertaken, may be dominated by interpolation effects rather than providing true images. We found that in this case, a presentation of the values in the complex plane (Argand diagram) is better suited to find common aspects in the data. Since no distinct features could be found in the range 10 s to 100 s, we concentrated our investigations mainly to the decade 100 s to 1000 s. The real and imaginary parts of the predicted values B_z^p of all sites at periods 450 s and 910 s are presented in Argand diagrams (Fig. 3) for 4 different polarizations of the event.

Varying the polarization of the hypothetical event moves the points in the complex plane relative to each other, according to the contribution of the regional vertical field. At a polarization azimuth of about $-30°$ the predicted values calculated from the observed response functions arrange approximately on a line through the origin. This happens when the hypothetic magnetic

Fig. 3. Hypothetical event analysis, Argand diagrams: Predicted vertical magnetic fields B_z^p of all sites at periods 450 s (upper half) and 910 s (lower half). RE: real parts, IM: imaginary parts. (a) Polarization azimuth of the hypothetical magnetic field (with amplitude = 1, phase = 0°) : $\vartheta^* = 0°$, (b) $\vartheta^* = 90°$, (c) $\vartheta^* = -30°$, (d) $\vartheta^* = 60°$.

field is polarized parallel to the strike direction of the regional structure, or is perpendicular to it. The strike angle can therefore be expected at $-30°$ or at $60°$. The latter corresponds well to the strike found by MT decomposition methods at $45°-60°$. The slope of the line through the origin was determined by weighted least squares fitting; it dips $-30°$ at 450 s and ca. $-20°$ at 910 s. The negative gradients indicate negative common phases, which can only be produced by mainly inductive processes. The phases vary consistently from $-40°$ to $-20°$ from shorter to longer periods. However, the optimum polarization azimuth is constantly $-30°$ throughout the investigated period range and can therefore be attributed to the strike direction of a more regional structure. Unfortunately, the errors of the response functions increase towards the long period end, so that no reliable results can be obtained from data beyond 1000 s.

4. Thin Sheet Modelling—The Deep Crustal Conductor

The method described above aims to recover regional two-dimensional information from an originally three-dimensional problem. It is therefore interesting to expand these investigations by some three-dimensional model calculations. Another question that arose from previous MT and GDS interpretations in the area is whether the deep crustal conductor is L-shaped (striking N/S and E/W), or whether it consists of two separate parts: one situated in the west and striking N/S, the other one located further east and striking NE/SW (the so-called SABC anomaly in Southern Alberta - British Columbia). A detailed description of the general geological situation of the area can be found in Jones (1993). We concentrate our efforts on the investigation of the induction arrows in the region of the BC87 profile (Fig. 4). The models are calculated with the McKirdy and Weaver thin sheet code (McKirdy et al., 1985) for a period of 1000 s.

The emphasis of such an investigation can only be to study principal effects, as the range of valid thin sheet models is limited by strict requirements for valid cell geometry and conductivity gradients (e.g., Weaver, 1994). Consequently, resistivity contrasts and sizes in our models are oversimplified. Both models in Fig. 4 rely on three principal cell resistivities. Cells of 250 Ω·m generally denote conductive material in a 500 Ω·m host, resistive cells of 750 Ω·m represent a more resistive region in association with the Nelson Batholith.

In both models, the magnetic response functions are clearly affected by the resistive complex and their induction arrows are attenuated over its centre. Along the edges of the resistor we find the greatest current concentrations and hence, the largest induction arrows. At the south-eastern part of the resistor, the arrows are also influenced by the form of the conductor. East of the batholith, the real arrows are bent into directions perpendicular to the strike of the 'second' conductor: near the E/W striking structure they point northwards, while arrows near the oblique conductor have a northwest tendency. However, across the southern part of the batholith, and in the vicinity south of it, the arrows point generally towards the northeastern direction in both models, although arrows of the SABC model in the southern area are clearly more inclined to the east. The main difference between the responses from the models is manifested in the lengths of the real arrows in the region east of the resistor. The arrows decrease towards the center of the SABC conductor and also reverse their sign beyond it, whereas they are of constant lengths along the edge of the L-shaped conductor. The imaginary arrows are generally smaller and point at varying, non-parallel angles relative to the real arrows due to the strong three-dimensionality of the studied area.

The azimuthal distribution of the BC87 data along the profile shows a preferred direction of the real arrows of approximately $10°$ to $30°$ from north, although directions of ca. $-20°$ occur as well at the more easterly located sites. The lengths of the real arrows decrease towards the east, and at the most eastern sites of the profile they point strictly westwards. Although the observed real arrows are generally longer than the modelled arrows, the general behaviour of arrow directions and magnitudes supports the oblique model.

Induction arrows (Wiese convention)

L-shaped model
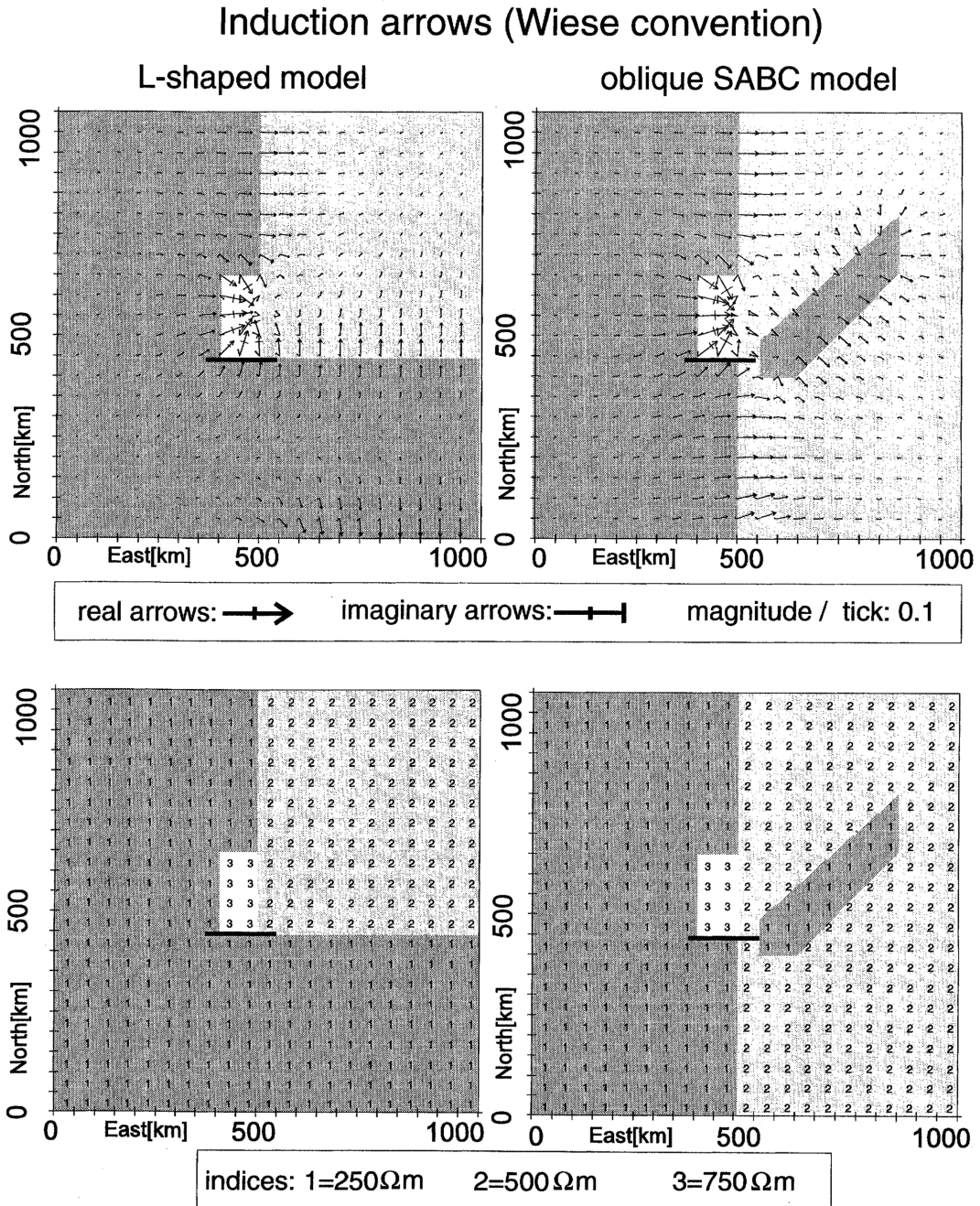
oblique SABC model

Fig. 4.　3-D thin sheet modelling of the deep crustal conductor: Induction arrows (Wiese convention) for the L-shaped model (left) and the oblique SABC model (right). Marked in the central parts of the figures are the resistor associated with the Nelson Batholith and the approximate location of the BC87 profile (thick line). The sheet cells extend to 50 km in each direction. Beneath the thin sheet we placed a resistive layer of 750 $\Omega \cdot$m which is followed by a homogeneous halfspace (50 $\Omega \cdot$m) at a depth of 400 km.

5. Conclusion

The GDS response functions of the BC87 dataset at long periods are affected by both local and regional induction processes. Since the directions of induction arrows are inconsistent with the regional strike directions found by MT decomposition methods, we applied hypothetical event analysis to the data. This technique is capable of recovering regional information that is common to all sites from the observed response functions. Although better quality of the data in the examined period range (100 s–1000 s) would be desirable, the predicted values for the vertical magnetic field at all sites reveal common phase angles for polarizations azimuths of around −30°. This azimuth corresponds to the strike of the regional conductivity structure or to a perpendicular direction.

Since the common phase angles are negative we must assume that large scale local structures, which may be associated with the resistive Nelson Batholith region, are responsible for contributions of more inductive rather than galvanic origin to the regional response functions. Due to the geological complexity of the region, the limited spatial coverage, and the deficient data quality at long periods, this dataset might not be appropriate to show the full capability of the method; however the regional strike found is in good agreement with the strike direction determined by decomposition of MT impedances at 45°–60°.

Thin sheet modelling studies of the deep crustal conductor (L-shaped or oblique) at 1000 s confirmed that induction arrows along the BC87 profile may generally be produced by current concentrations around the area that is associated with the resistive Nelson Batholith. Only sites in the (south-) eastern part of the batholith are affected by the form of the deep crustal conductor. The azimuth distributions and the length variations of the real arrows in the area of the profile indicate that the observed data may rather represent the oblique model (SABC conductor). Also, the direction of the SABC conductor could possibly explain the azimuth of the regional strike found by hypothetical event analysis.

REFERENCES

Chave, A. D. and J. T. Smith, On electric and magnetic galvanic distortion tensor decompositions, *J. Geophys. Res.*, **99 B3**, 4669–4682, 1994.

DeGroot-Hedlin, C., Inversion for regional 2-D resistivity structure in the presence of galvanic scatterers, *Geophys. J. Int.*, **122**, 877–888, 1995.

Eisel, M. and K. Bahr, Electrical anisotropy in the lower crust of British-Columbia—an interpretation of a magnetotelluric profile after tensor decomposition, *J. Geomag. Geoelectr.*, **45**, 1115–1126, 1993.

Groom, R. W., The effects of inhomogeneities on magnetotellurics, Ph.D. thesis, Univ. Toronto, 1988.

Jones, A. G., The BC87 dataset—tectonic setting, previous EM results, and recorded MT data, *J. Geomag. Geoelectr.*, **45**, 1089–1105, 1993.

Jones, A. G., R. W. Groom, and R. D. Kurtz, Decomposition and modelling of the BC87 dataset, *J. Geomag. Geoelectr.*, **45**, 1127–1150, 1993.

McKirdy, D. M., J. T. Weaver, and T. W. Dawson, Induction in a thin sheet of variable conductance at the surface of a stratified Earth—II. Three-dimensional theory, *Geophys. J. R. astr. Soc.*, **80**, 177–194, 1985.

Ritter, P., Separation of local and regional information in geomagnetic response functions using hypothetical event analysis, Ph.D. Thesis, Univ. of Edinburgh, 1996.

Weaver, J. T., *Mathematical Methods for Geo-Electromagnetic Induction*, Research Studies Press, Taunton, England, 1994.

Zhang, P., L. B. Pedersen, M. Mareschal, and M. Chouteau, Channelling contribution to tipper vectors: a magnetic equivalent to electrical distortion, *Geophys. J. Int.*, **113**, 693–700, 1993.